

# Buckling of sandwich plates with FG-CNT-reinforced layers resting on orthotropic elastic medium using Reddy plate theory

Maryam Shokravi\*

Buein Zahra Technical University, Buein Zahra, Qazvin, Iran

(Received October 19, 2016, Revised February 10, 2017, Accepted February 14, 2017)

**Abstract.** Present paper deals with the temperature-dependent buckling analysis of sandwich nanocomposite plates resting on elastic medium subjected to magnetic field. The lamina layers are reinforced with carbon nanotubes (CNTs) as uniform and functionally graded (FG). The elastic medium is considered as orthotropic Pasternak foundation with considering the effects of thermal loading on the spring and shear constants of medium. Mixture rule is utilized for obtaining the effective material properties of each layer. Adopting the Reddy shear deformation plate theory, the governing equations are derived based on energy method and Hamilton's principle. The buckling load of the structure is calculated with the Navier's method for the simply supported sandwich nanocomposite plates. Parametric study is conducted on the combined effects of the volume percent and distribution types of the CNTs, temperature change, elastic medium, magnetic field and geometrical parameters of the plates on the buckling load of the sandwich structure. The results show that FGX distribution of the CNTs leads to higher stiffness and consequently higher buckling load. In addition, considering the magnetic field increases the buckling load of the sandwich nanocomposite plate.

**Keywords:** buckling of sandwich nanocomposite plates; magnetic field; FG-CNT; temperature-dependent; Reddy shear deformation plate theory

## 1. Introduction

The application and using from laminated composites structure in different industries such as aerospace, automobile and etc is growing. It is due to the fact that in the laminated composites structure, the strength with respect to the weight is high and however, these materials can improve the stability of structure and decrease the weight of system. So in recent years, the study and mechanical analysis of the laminated composites structure have been intense interests the researchers. In this paper, the laminas are reinforced with CNT which can increase the stiffness of the structure.

Mechanical analysis of laminated plates has been investigated by many authors. Free vibration of laminated plates was addressed by Gupta *et al.* (2003) to show the capability of the present method in the vicinity of higher order shear deformation theory and simply supported edges of plates. Lee and Park (2007) investigated buckling behaviors of laminated composite structures with a delamination using the enhanced assumed strain (EAS) solid element. The EAS three-dimensional finite element (FE) formulation was described. Dash and Singh (2012) addressed the buckling and post-buckling of laminated composite plates using higher order shear deformation theory associated with Green-Lagrange non-linear strain-

displacement relationships. Buckling analysis of laminated composite plates was carried out by Singh and Chakrabarti (2012) using an efficient C0 FE model developed based on higher order zigzag theory. In this model the first derivatives of transverse displacement have been treated as independent variables to overcome the problem of C1 continuity associated with the FE implementation of the plate theory. Static and dynamic characteristics of composite plates subjected to an arbitrary periodic load in hygrothermal environments were presented by Wang *et al.* (2013). Meshless collocations utilizing Gaussian and Multiquadric radial basis functions for the stability analysis of orthotropic and cross ply laminated composite plates subjected to thermal and mechanical loading were presented by Singh *et al.* (2013). The material properties of composite plates were depended on the temperature and moisture. Chen *et al.* (2013) studied the dynamic instability of laminated composite plates under thermal and arbitrary in-plane periodic loads using first-order shear deformation plate theory. Based on Bolotin's method, the system equations of Mathieu-type were formulated and used to determine dynamic instability regions of laminated plates in the thermal environment. Buckling and vibration characteristics of circular laminated plates under in-plane edge loads and resting on Winkler-type foundation were solved by Afsharmanesh *et al.* (2014) using Ritz method. The effects of fiber orientation on the natural frequencies and critical buckling loads of laminated angle-ply plates were studied. Chaotic motion in a nonlinear laminated composite plate under subsonic fluid flow and a simultaneous external load was studied by Norouzi and

---

\*Corresponding author, Ph.D.,  
E-mail: [Maryamshokravi10@gmail.com](mailto:Maryamshokravi10@gmail.com);  
[Maryamshokravi10@bzte.ac.ir](mailto:Maryamshokravi10@bzte.ac.ir)

Younesian (2016) based on Melnikov's integral approach. Javed *et al.* (2016) analyzed vibration of anti-symmetric angle-ply plates using spline method for higher order shear theory.

None of the above mentioned works have been considered nanocomposite structures. In this regards, within the framework of classical beam theory, Yas and Heshmati (2012) studied of the vibrational properties of FG nanocomposite beams reinforced by randomly oriented straight single-walled carbon nanotubes (SWCNTs) under the actions of moving load. Timoshenko and Euler-Bernoulli beam theories were used to evaluate dynamic characteristics of the beam. Yang *et al.* (2015) investigated the dynamic buckling behavior of FG-CNT-reinforced integrated with two surface bonded piezoelectric layers. Geometrically nonlinear large deformation analysis of FG-CNT-reinforced composite skew plates was presented by Zhang and Liew (2015). Bending, buckling and free vibration behaviors of functionally graded (FG) carbon nanotube (CNT)-reinforced polymer composite beam under different non-uniform thermal loads were analyzed by Mayandi and Jeyaraj (2015) using finite element method.

They showed that the fundamental buckling mode shape was not sensitive to the nature of temperature variation but bending amplitude of the buckling mode shape is significantly influenced by functional grading of CNT and volume fraction of the CNT. Parametric studies were conducted to examine the effects of CNT content by volume, elastic foundation, skew angle, plate width-to-thickness ratio, plate aspect ratio and boundary conditions on the nonlinear responses of the FG-CNT reinforced composite skew plates. Kolahchi *et al.* (2015) studied nonlinear buckling analysis of embedded polymeric temperature-dependent microplates. Their results indicate that the buckling load increases with increasing magnetic field. Lei *et al.* (2016a, b) considered the free vibration and buckling behaviors of FG-CNT-reinforced composite thick straight-sided quadrilateral plates resting on Pasternak foundations based on Ritz method. The first-order shear deformation theory (FSDT) was employed for formulation of the energy functional to incorporate the effects of transverse shear deformation and rotary inertia. Temperature-dependent nonlinear dynamic stability of FG-CNT-reinforced visco-plate was present by Kolahchi *et al.*

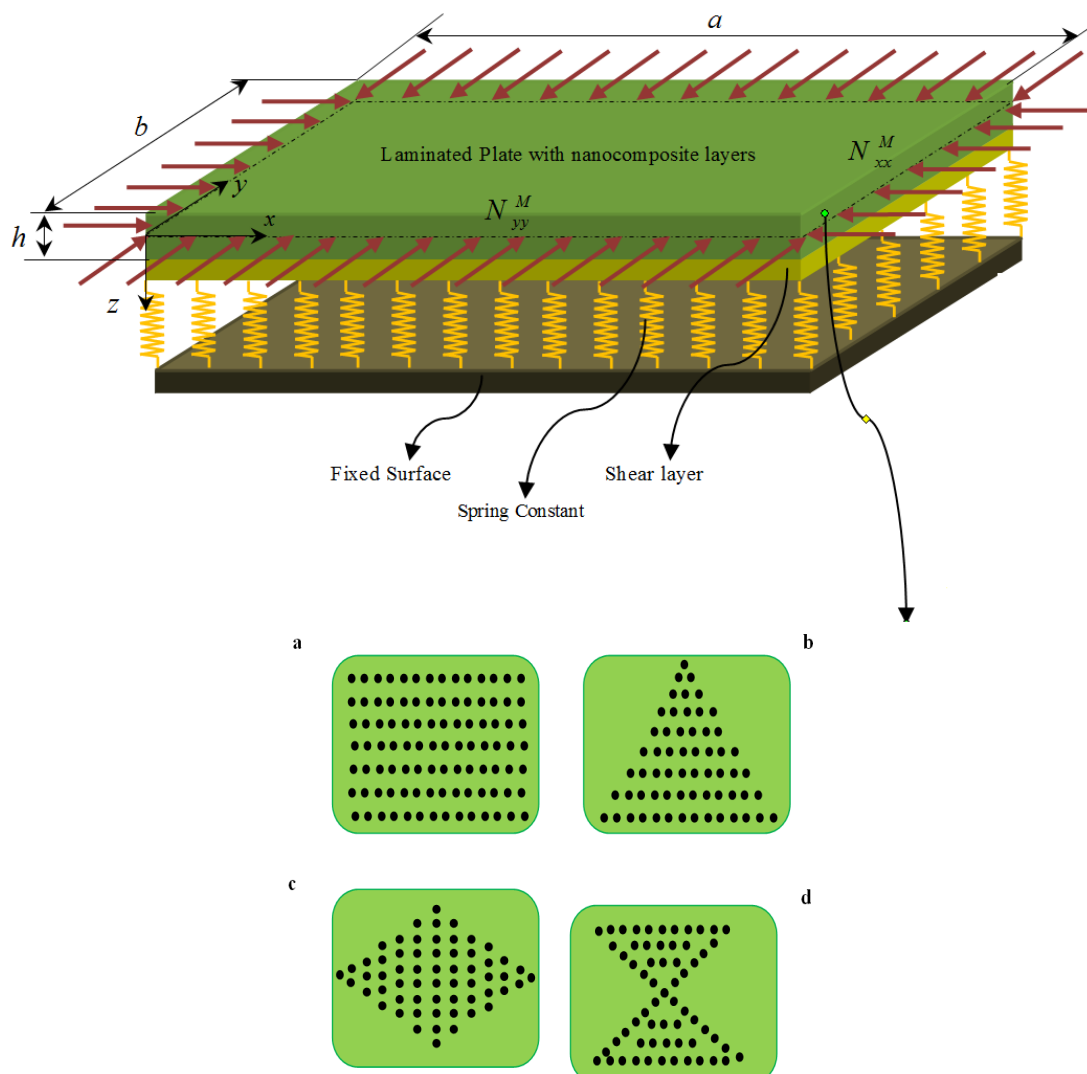


Fig. 1 The sandwich plate with FG-CNT-reinforced layers resting on elastic foundation

(2016). They showed that the lowest and highest dynamic instability region were respectively obtained for FGX- and FGO-CNTRC viscoplates. Kiani (2016) obtained the buckling loads and buckling pattern of composite plates reinforced with carbon nanotubes with uniform or functionally graded distribution across the plate thickness. Using the Ritz method and Airy stress function formulation, the distribution of stress resultants in the plate domain was obtained as a two-dimensional elasticity formulation. Vibration analysis of embedded functionally graded (FG)-carbon nanotubes (CNT)-reinforced piezoelectric cylindrical shell subjected to uniform and non-uniform temperature distributions were presented by Madani *et al.* (2016) using differential cubature (DC) method.

However, the buckling analysis of sandwich nanocomposite plates has not been studied by researchers. In this paper, buckling load of the sandwich plates with FG-CNT-reinforced layers is obtained based on Reddy shear deformation plate theory. The material properties of the plates and constants of elastic medium are assumed temperature-dependent. Mixture rule is utilized for calculating the equivalent characteristic of the nanocomposite structure. The effects of different parameters such as volume percent and distribution types of the CNTs, temperature change, elastic medium, magnetic field and geometrical parameters of the plates on the buckling load of the sandwich structure are shown on the buckling behaviour of the structure.

## 2. Formulation

A sandwich plate with FG-CNT-reinforced layers resting on elastic medium is shown in Fig. 1 with length  $a$ , width  $b$  and thickness  $h$ .

### 2.1 Reddy plate theory

In the Reddy plate theory, the displacement field is a cubic function of  $z$  and transverse shear stresses are the functions of second order. However, the displacement field of this theory can be written as (Reddy 1984)

$$U(x, y, z, t) = u(x, y, t) + z\phi_x(x, y, t) + c_1 z^3 \left( \phi_x + \frac{\partial w}{\partial x} \right), \quad (1)$$

$$V(x, y, z, t) = v(x, y, t) + z\phi_y(x, y, t) + c_1 z^3 \left( \phi_y + \frac{\partial w}{\partial y} \right), \quad (2)$$

$$W(x, y, z, t) = w(x, y, t), \quad (3)$$

where  $u$ ,  $v$  and  $w$  are the displacement components of the mid-plane and  $\phi_x$ ,  $\phi_y$  are the angle of rotation around the  $y$  and  $x$  axes of cross-section, respectively. Also  $c_1 = -4/3h^2$  in which  $h$  is the thickness of the plate. So the kinematic relations are defined as follows

$$\begin{pmatrix} \varepsilon_{xx} \\ \varepsilon_{yy} \\ \gamma_{xy} \end{pmatrix} = \begin{pmatrix} \varepsilon_{xx}^0 \\ \varepsilon_{yy}^0 \\ \gamma_{xy}^0 \end{pmatrix} + z \begin{pmatrix} \varepsilon_{xx}^1 \\ \varepsilon_{yy}^1 \\ \gamma_{xy}^1 \end{pmatrix} + z^3 \begin{pmatrix} \varepsilon_{xx}^3 \\ \varepsilon_{yy}^3 \\ \gamma_{xy}^3 \end{pmatrix}, \quad (4)$$

$$\begin{pmatrix} \gamma_{yz} \\ \gamma_{xz} \end{pmatrix} = \begin{pmatrix} \gamma_{yz}^0 \\ \gamma_{xz}^0 \end{pmatrix} + z^2 \begin{pmatrix} \gamma_{yz}^2 \\ \gamma_{xz}^2 \end{pmatrix}, \quad (5)$$

in which

$$\begin{pmatrix} \varepsilon_{xx}^0 \\ \varepsilon_{yy}^0 \\ \gamma_{xy}^0 \end{pmatrix} = \begin{pmatrix} \frac{\partial u}{\partial x} \\ \frac{\partial v}{\partial y} \\ \frac{\partial u}{\partial y} + \frac{\partial v}{\partial x} \end{pmatrix}, \quad \begin{pmatrix} \varepsilon_{xx}^1 \\ \varepsilon_{yy}^1 \\ \gamma_{xy}^1 \end{pmatrix} = \begin{pmatrix} \frac{\partial \phi_x}{\partial x} \\ \frac{\partial \phi_y}{\partial y} \\ \frac{\partial \phi_x}{\partial y} + \frac{\partial \phi_y}{\partial x} \end{pmatrix}, \quad (6)$$

$$\begin{pmatrix} \varepsilon_{xx}^3 \\ \varepsilon_{yy}^3 \\ \gamma_{xy}^3 \end{pmatrix} = c_1 \begin{pmatrix} \frac{\partial \phi_x}{\partial x} + \frac{\partial^2 w}{\partial x^2} \\ \frac{\partial \phi_y}{\partial y} + \frac{\partial^2 w}{\partial y^2} \\ \frac{\partial \phi_x}{\partial y} + \frac{\partial \phi_y}{\partial x} + 2 \frac{\partial^2 w}{\partial x \partial y} \end{pmatrix},$$

$$\begin{pmatrix} \gamma_{yz}^0 \\ \gamma_{xz}^0 \end{pmatrix} = \begin{pmatrix} \phi_y + \frac{\partial w}{\partial y} \\ \phi_x + \frac{\partial w}{\partial x} \end{pmatrix}, \quad \begin{pmatrix} \gamma_{yz}^2 \\ \gamma_{xz}^2 \end{pmatrix} = c_2 \begin{pmatrix} \phi_y + \frac{\partial w}{\partial y} \\ \phi_x + \frac{\partial w}{\partial x} \end{pmatrix}, \quad (7)$$

where  $c_2 = 3c_1$ . Based on this theory, the stress-strain relations can be written using Hook's law as follows

$$\begin{pmatrix} \sigma_{xx} \\ \sigma_{yy} \\ \sigma_{xy} \\ \sigma_{xz} \\ \sigma_{yz} \end{pmatrix} = \begin{bmatrix} Q_{11} & Q_{12} & 0 & 0 & 0 \\ Q_{12} & Q_{22} & 0 & 0 & 0 \\ 0 & 0 & Q_{66} & 0 & 0 \\ 0 & 0 & 0 & Q_{55} & 0 \\ 0 & 0 & 0 & 0 & Q_{44} \end{bmatrix} \begin{pmatrix} \varepsilon_{xx} - \alpha_{xx} T \\ \varepsilon_{yy} - \alpha_{yy} T \\ \gamma_{xy} \\ \gamma_{xz} \\ \gamma_{yz} \end{pmatrix}, \quad (8)$$

where  $\alpha_{xx}$ ,  $\alpha_{yy}$  and  $T$  are thermal expansion and temperature change, respectively;  $Q_{ij}$  ( $i, j = 1, 2, \dots, 6$ ) denotes elastic coefficients which can be obtained by Mixture rule.

### 2.2 Mixture rule

According to this theory, the effective Young and shear moduli of structure may be expressed as (Zhang and Liew 2015)

$$E_{11} = \eta_1 V_{CNT} E_{r11} + (1 - V_{CNT}) E_m, \quad (9)$$

$$\frac{\eta_2}{E_{22}} = \frac{V_{CNT}}{E_{r22}} + \frac{(1 - V_{CNT})}{E_m}, \quad (10)$$

$$\frac{\eta_3}{G_{12}} = \frac{V_{CNT}}{G_{r12}} + \frac{(1 - V_{CNT})}{G_m}, \quad (11)$$

where  $E_{r11}$ ,  $E_{r22}$  and  $E_m$  are Young's moduli of CNTs and matrix, respectively;  $G_{r11}$  and  $G_m$  are shear modulus of CNTs and matrix, respectively;  $V_{CNT}$  and  $V_m$  show the volume fractions of the CNTs and matrix, respectively;  $\eta_j$  ( $j = 1, 2, 3$ ) is CNT efficiency parameter for considering the size-dependent material properties. Noted that this para-

meter may be calculated using molecular dynamic (MD). However, the CNT distribution for the mentioned patterns obeys from the following relations (Zhang and Liew 2015)

$$UD: V_{CNT} = V_{CNT}^*, \quad (12)$$

$$FGV: V_{CNT}(z) = \left(1 + \frac{2z}{h}\right) V_{CNT}^*, \quad (13)$$

$$FGO: V_{CNT}(z) = 2 \left(1 - \frac{2|z|}{h}\right) V_{CNT}^*, \quad (14)$$

$$FGX: V_{CNT}(z) = 2 \left(\frac{2|z|}{h}\right) V_{CNT}^*, \quad (15)$$

Furthermore, the thermal expansion coefficients in the axial and transverse directions respectively ( $\alpha_{11}$  and  $\alpha_{22}$ ) and the density ( $\rho$ ) of the nano-composite structure can be written as

$$\rho = V_{CNT} \rho_r + V_m \rho_m, \quad (16)$$

$$\alpha_{11} = V_{CNT} \alpha_{r11} + V_m \alpha_m, \quad (17)$$

$$\alpha_{22} = (1 + \nu_{r12}) V_{CNT} \alpha_{r22} + (1 + \nu_m) V_m \alpha_m - \nu_{12} \alpha_{11}, \quad (18)$$

where

$$V_{CNT}^* = \frac{w_{CNT}}{w_{CNT} + (\rho_{CNT} / \rho_m) - (\rho_{CNT} / \rho_m) w_{CNT}}, \quad (19)$$

where  $w_{CNT}$  is the mass fraction of the CNT;  $\rho_m$  and  $\rho_{CNT}$  present the densities of the matrix and CNT, respectively;  $\nu_{r12}$  and  $\nu_m$  are Poisson's ratios of the CNT and matrix, respectively;  $\alpha_{r11}$ ,  $\alpha_{r22}$  and  $\alpha_m$  are the thermal expansion coefficients of the CNT and matrix, respectively. Noted that  $\nu_{12}$  is assumed as constant.

### 2.3 Energy method

The strain energy of the structure can be written as

$$U = \frac{1}{2} \int_{\Omega_0} \int_{-h/2}^{h/2} (\sigma_{xx} \varepsilon_{xx} + \sigma_{yy} \varepsilon_{yy} + \sigma_{xy} \gamma_{xy} + \sigma_{xz} \gamma_{xz} + \sigma_{yz} \gamma_{yz}) dV. \quad (20)$$

Substituting Eqs. (4) and (5) into Eq. (20) yields

$$U = \frac{1}{2} \int_0^b \int_0^a \left[ N_{xx} \left( \frac{\partial u}{\partial x} \right) + N_{yy} \left( \frac{\partial v}{\partial y} \right) + Q_{yy} \left( \frac{\partial w}{\partial y} + \phi_y \right) + Q_{xx} \left( \frac{\partial w}{\partial x} + \phi_x \right) + N_{xy} \left( \frac{\partial v}{\partial x} + \frac{\partial u}{\partial y} \right) + M_{xx} \frac{\partial \phi_x}{\partial x} + M_{yy} \frac{\partial \phi_y}{\partial y} + M_{xy} \left( \frac{\partial \phi_x}{\partial y} + \frac{\partial \phi_y}{\partial x} \right) + K_{yy} \left( c_2 \left( \phi_y + \frac{\partial w}{\partial y} \right) \right) + K_{xx} \left( c_2 \left( \phi_x + \frac{\partial w}{\partial x} \right) \right) \right] dx dy \quad (21)$$

$$+ P_{xx} \left( c_1 \left( \frac{\partial \phi_x}{\partial x} + \frac{\partial^2 w}{\partial x^2} \right) \right) + P_{yy} \left( c_1 \left( \frac{\partial \phi_y}{\partial y} + \frac{\partial^2 w}{\partial y^2} \right) \right) + P_{xy} \left( \frac{\partial \phi_y}{\partial x} + \frac{\partial \phi_x}{\partial y} + 2 \frac{\partial^2 w}{\partial x \partial y} \right) dx dy \quad (21)$$

where the stress resultants can be defined as

$$\left[ (N_{xx}, N_{yy}, N_{xy}), (M_{xx}, M_{yy}, M_{xy}), (P_{xx}, P_{yy}, P_{xy}) \right] = \int_{-h/2}^{h/2} \begin{bmatrix} \sigma_{xx} \\ \sigma_{yy} \\ \sigma_{xy} \end{bmatrix} [1, z, z^3] dz, \quad (22)$$

$$\left[ (Q_{xx}, Q_{yy}), (K_{xx}, K_{yy}) \right] = \int_{-h/2}^{h/2} \begin{bmatrix} \sigma_{xz} \\ \sigma_{yz} \end{bmatrix} [1, z^2] dz, \quad (23)$$

The work due to the in-plane external loads, elastic medium and magnetic field can be expressed as (Madani *et al.* 2016, Kolahchi *et al.* 2016b, c)

$$W = -\frac{1}{2} \int_0^b \int_0^a \left[ (N_{xx}^M + N_{xx}^T) \left( \frac{\partial w}{\partial x} \right)^2 + (N_{yy}^M + N_{yy}^T) \left( \frac{\partial w}{\partial y} \right)^2 \right] dx dy - \frac{1}{2} \int_0^b \int_0^a \left[ \eta H_x^2 \frac{\partial^2 w}{\partial x^2} \right] dx dy - \frac{1}{2} \int_0^b \int_0^a \left[ -K_w w + G_\xi \left( \cos^2 \theta \frac{\partial^2 w}{\partial x^2} + 2 \cos \theta \sin \theta \frac{\partial^2 w}{R \partial x \partial \theta} + \sin^2 \theta \frac{\partial^2 w}{R^2 \partial \theta^2} \right) + G_\eta \left( \sin^2 \theta \frac{\partial^2 w}{\partial x^2} - 2 \sin \theta \cos \theta \frac{\partial^2 w}{R \partial x \partial \theta} + \cos^2 \theta \frac{\partial^2 w}{R^2 \partial \theta^2} \right) \right] dx dy, \quad (24)$$

where  $K_w$  and  $G_\xi$ ,  $G_\eta$  are Winkler's spring modulus and shear layer coefficients, respectively. In addition, angle  $\theta$  describes the local  $\xi$  direction of orthotropic foundation with respect to the global  $x$ -axis of the plate;  $\eta$  is the magnetic permeability and  $H_x$  is the magnetic field. Also  $N_{xx}^M = -p$  and  $N_{yy}^M = \alpha N_{xx}^M$  are applied loads to the plate in  $x$  and  $y$  directions, respectively and  $\alpha$  is a constant coefficient. In addition,  $N_{\theta\theta}^T$ ,  $N_{xx}^T$  are thermal forces which may be written as

$$\begin{Bmatrix} N_{xx}^T \\ N_{\theta\theta}^T \end{Bmatrix} = \int_{-h/2}^{h/2} \begin{Bmatrix} C_{11}(T, z) \alpha_{xx}(z) + C_{12}(T, z) \alpha_{\theta\theta}(z) \\ C_{12}(T, z) \alpha_{xx}(z) + C_{22}(T, z) \alpha_{\theta\theta}(z) \end{Bmatrix} \Delta T dz. \quad (25)$$

The governing equations can be derived by Hamilton's principal as follows

$$\delta u : \frac{\partial N_{xx}}{\partial x} + \frac{\partial N_{xy}}{\partial y} = 0, \quad (26)$$

$$\delta v : \frac{\partial N_{xy}}{\partial x} + \frac{\partial N_{yy}}{\partial y} = 0, \quad (27)$$

$$\begin{aligned} \delta w : & \frac{\partial Q_{xx}}{\partial x} + \frac{\partial Q_{yy}}{\partial y} + c_2 \left( \frac{\partial K_{xx}}{\partial x} + \frac{\partial K_{yy}}{\partial y} \right) \\ & + (N_{xx}^M + N_{xx}^T) \frac{\partial^2 w}{\partial x^2} + (N_{yy}^M + N_{yy}^T) \frac{\partial^2 w}{\partial y^2} \\ & - c_1 \left( \frac{\partial^2 P_{xx}}{\partial x^2} + 2 \frac{\partial^2 P_{xy}}{\partial x \partial y} + \frac{\partial^2 P_{yy}}{\partial y^2} \right) - K_w w \\ & + G_\xi \left( \cos^2 \theta \frac{\partial^2 w}{\partial x^2} + 2 \cos \theta \sin \theta \frac{\partial^2 w}{R \partial x \partial \theta} \right. \\ & \left. + \sin^2 \theta \frac{\partial^2 w}{R^2 \partial \theta^2} \right) + G_\eta \left( \sin^2 \theta \frac{\partial^2 w}{\partial x^2} \right. \\ & \left. - 2 \sin \theta \cos \theta \frac{\partial^2 w}{R \partial x \partial \theta} + \cos^2 \theta \frac{\partial^2 w}{R^2 \partial \theta^2} \right) \\ & + \eta h H_x^2 \frac{\partial^2 w}{\partial x^2} = 0, \quad (28) \end{aligned}$$

$$\delta \phi_x : \frac{\partial M_{xx}}{\partial x} + \frac{\partial M_{xy}}{\partial y} + c_1 \left( \frac{\partial P_{xx}}{\partial x} + \frac{\partial P_{xy}}{\partial y} \right) - Q_{xx} - c_2 K_{xx} = 0, \quad (29)$$

$$\delta \phi_y : \frac{\partial M_{xy}}{\partial x} + \frac{\partial M_{yy}}{\partial y} + c_1 \left( \frac{\partial P_{xy}}{\partial x} + \frac{\partial P_{yy}}{\partial y} \right) - Q_{yy} - c_2 K_{yy} = 0. \quad (30)$$

Combining Eqs. (4)-(8), (22) and (23), the stress resultants can be obtained as follows

$$\begin{aligned} N_{xx} = & A_{11} \frac{\partial u}{\partial x} + A_{12} \frac{\partial v}{\partial y} + B_{11} \frac{\partial \phi_x}{\partial x} + B_{12} \frac{\partial \phi_y}{\partial y} \\ & + E_{11} c_1 \left( \frac{\partial \phi_x}{\partial x} + \frac{\partial^2 w}{\partial x^2} \right) + E_{12} c_1 \left( \frac{\partial \phi_y}{\partial y} + \frac{\partial^2 w}{\partial y^2} \right), \quad (31) \end{aligned}$$

$$\begin{aligned} N_{yy} = & A_{12} \frac{\partial u}{\partial x} + A_{22} \frac{\partial v}{\partial y} + B_{12} \frac{\partial \phi_x}{\partial x} + B_{22} \frac{\partial \phi_y}{\partial y} \\ & + E_{12} c_1 \left( \frac{\partial \phi_x}{\partial x} + \frac{\partial^2 w}{\partial x^2} \right) + E_{22} c_1 \left( \frac{\partial \phi_y}{\partial y} + \frac{\partial^2 w}{\partial y^2} \right), \quad (32) \end{aligned}$$

$$\begin{aligned} N_{xy} = & A_{66} \left( \frac{\partial u}{\partial y} + \frac{\partial v}{\partial x} \right) + B_{66} \left( \frac{\partial \phi_x}{\partial y} + \frac{\partial \phi_y}{\partial x} \right) \\ & + E_{66} c_1 \left( \frac{\partial \phi_y}{\partial x} + \frac{\partial \phi_x}{\partial y} + 2 \frac{\partial^2 w}{\partial x \partial y} \right), \quad (33) \end{aligned}$$

$$M_{xx} = B_{11} \frac{\partial u}{\partial x} + B_{12} \frac{\partial v}{\partial y} + D_{11} \frac{\partial \phi_x}{\partial x} + D_{12} \frac{\partial \phi_y}{\partial y} \quad (34)$$

$$+ F_{11} c_1 \left( \frac{\partial \phi_x}{\partial x} + \frac{\partial^2 w}{\partial x^2} \right) + F_{12} c_1 \left( \frac{\partial \phi_y}{\partial y} + \frac{\partial^2 w}{\partial y^2} \right), \quad (34)$$

$$\begin{aligned} M_{yy} = & B_{12} \frac{\partial u}{\partial x} + B_{22} \frac{\partial v}{\partial y} + D_{12} \frac{\partial \phi_x}{\partial x} + D_{22} \frac{\partial \phi_y}{\partial y} \\ & + F_{12} c_1 \left( \frac{\partial \phi_x}{\partial x} + \frac{\partial^2 w}{\partial x^2} \right) + F_{22} c_1 \left( \frac{\partial \phi_y}{\partial y} + \frac{\partial^2 w}{\partial y^2} \right), \quad (35) \end{aligned}$$

$$\begin{aligned} M_{xy} = & B_{66} \left( \frac{\partial u}{\partial y} + \frac{\partial v}{\partial x} \right) + D_{66} \left( \frac{\partial \phi_x}{\partial y} + \frac{\partial \phi_y}{\partial x} \right) \\ & + F_{66} c_1 \left( \frac{\partial \phi_y}{\partial x} + \frac{\partial \phi_x}{\partial y} + 2 \frac{\partial^2 w}{\partial x \partial y} \right), \quad (36) \end{aligned}$$

$$\begin{aligned} P_{xx} = & E_{11} \frac{\partial u}{\partial x} + E_{12} \frac{\partial v}{\partial y} + F_{11} \frac{\partial \phi_x}{\partial x} + F_{12} \frac{\partial \phi_y}{\partial y} \\ & + H_{11} c_1 \left( \frac{\partial \phi_x}{\partial x} + \frac{\partial^2 w}{\partial x^2} \right) + H_{12} c_1 \left( \frac{\partial \phi_y}{\partial y} + \frac{\partial^2 w}{\partial y^2} \right), \quad (37) \end{aligned}$$

$$\begin{aligned} P_{yy} = & E_{12} \frac{\partial u}{\partial x} + E_{22} \frac{\partial v}{\partial y} + F_{12} \frac{\partial \phi_x}{\partial x} + F_{22} \frac{\partial \phi_y}{\partial y} \\ & + H_{12} c_1 \left( \frac{\partial \phi_x}{\partial x} + \frac{\partial^2 w}{\partial x^2} \right) + H_{22} c_1 \left( \frac{\partial \phi_y}{\partial y} + \frac{\partial^2 w}{\partial y^2} \right), \quad (38) \end{aligned}$$

$$\begin{aligned} P_{xy} = & E_{66} \left( \frac{\partial u}{\partial y} + \frac{\partial v}{\partial x} \right) + F_{66} \left( \frac{\partial \phi_x}{\partial y} + \frac{\partial \phi_y}{\partial x} \right) \\ & + H_{66} c_1 \left( \frac{\partial \phi_y}{\partial x} + \frac{\partial \phi_x}{\partial y} + 2 \frac{\partial^2 w}{\partial x \partial y} \right), \quad (39) \end{aligned}$$

$$Q_{xx} = A_{55} \left( \frac{\partial w}{\partial x} + \phi_x \right) + D_{55} c_2 \left( \phi_x + \frac{\partial w}{\partial x} \right), \quad (40)$$

$$Q_{yy} = A_{44} \left( \frac{\partial w}{\partial y} + \phi_y \right) + D_{44} c_2 \left( \frac{\partial w}{\partial y} + \phi_y \right), \quad (41)$$

$$K_{xx} = D_{55} \left( \frac{\partial w}{\partial x} + \phi_x \right) + F_{55} c_2 \left( \phi_x + \frac{\partial w}{\partial x} \right), \quad (42)$$

$$K_{yy} = D_{45} \left( \frac{\partial w}{\partial y} + \phi_y \right) + F_{44} c_2 \left( \frac{\partial w}{\partial y} + \phi_y \right), \quad (43)$$

where

$$\begin{aligned} & (A_{ij}, B_{ij}, D_{ij}, B_{ij}, F_{ij}, H_{ij}) \\ & = \sum_{k=1}^N \int_{z^{(k-1)}}^{z^{(k)}} Q_{ij}^{(k)} (1, z, z^2, z^3, z^4, z^6) dz, \quad (44) \\ & (i, j = 1, 2, 6) \end{aligned}$$

In which  $N$  is the number of sandwich plate layers. Finally the governing equations are obtained by substituting Eqs. (31)-(43) into governing equations (Eqs. (26)-(30)).

### 3. Solution method

Here, the Navier method is used for obtaining the buckling load of the sandwich structure for the simply supported boundary conditions. However, the displacement of the structure can be written as (Akhavan *et al.* 2009)

$$u(x, y) = \sum_{m=1}^{\infty} \sum_{n=1}^{\infty} u_{mn} \cos\left(\frac{m\pi x}{a}\right) \sin\left(\frac{n\pi y}{b}\right), \quad (45)$$

$$v(x, y) = \sum_{m=1}^{\infty} \sum_{n=1}^{\infty} v_{mn} \sin\left(\frac{m\pi x}{a}\right) \cos\left(\frac{n\pi y}{b}\right), \quad (46)$$

$$w(x, y) = \sum_{m=1}^{\infty} \sum_{n=1}^{\infty} w_{mn} \sin\left(\frac{m\pi x}{a}\right) \sin\left(\frac{n\pi y}{b}\right), \quad (47)$$

$$\phi_x(x, y) = \sum_{m=1}^{\infty} \sum_{n=1}^{\infty} \phi_{xmn} \cos\left(\frac{m\pi x}{a}\right) \sin\left(\frac{n\pi y}{b}\right), \quad (48)$$

$$\phi_y(x, y) = \sum_{m=1}^{\infty} \sum_{n=1}^{\infty} \phi_{ymn} \sin\left(\frac{m\pi x}{a}\right) \cos\left(\frac{n\pi y}{b}\right), \quad (49)$$

in which  $m$  and  $n$  are the wave numbers in  $x$  and  $y$  axes, respectively. Substituting Eqs. (45)-(49) into governing equations yields

$$[K] + p[K_G] = [0], \quad (50)$$

where  $[K]$  and  $[K_G]$  are stiffness and geometric matrixes, respectively. Finally, buckling load of the system ( $P$ ) can be calculated by using eigenvalue problem which is discussed in the next section.

### 4. Numerical results

In this section, the numerical results of buckling analysis of FG-CNT-reinforced sandwich plates resting on an orthotropic temperature-dependent elastic foundation are presented. Each layers of the sandwich structure are made from Poly methyl methacrylate (PMMA) with the constant Poisson's ratios of  $\nu_m = 0.34$ , temperature-dependent thermal coefficient of  $\alpha_m = (1 + 0.0005\Delta T) \times 10^{-6} / K$ , and temperature-dependent Young moduli of  $E_m = (3.52 - 0.0034T)$  GPa in which  $T = T_0 + \Delta T$  and  $T_0 = 300$  K (room temperature). CNTs as reinforcement of the lamina layers have the material properties listed in Table 1 (Zhang and Liew 2015). Since the surrounding medium is relatively soft, the foundation stiffness  $K_w$  may be expressed by (Zhang and Liew 2015)

$$K_w = \frac{E_0}{4L(1 - \nu_0^2)(2 - c_1)^2} \quad (51)$$

$$\left[5 - (2\gamma_1^2 + 6\gamma_1 + 5)\exp(-2\gamma_1)\right], \quad (51)$$

where

$$c_1 = (\gamma_1 + 2)\exp(-\gamma_1), \quad (52)$$

$$\gamma_1 = \frac{H_s}{L}, \quad (53)$$

$$E_0 = \frac{E_s}{(1 - \nu_s^2)}, \quad (54)$$

$$\nu_0 = \frac{\nu_s}{(1 - \nu_s)}, \quad (55)$$

where  $E_s$ ,  $\nu_s$ ,  $H_s$  are Young's modulus, Poisson's ratio and depth of the foundation, respectively. In this paper,  $E_s$  is assumed to be temperature-dependent while  $\nu_s$  is assumed to be a constant. The elastic medium is made of Poly dimethylsiloxane (PDMS) which the temperature-dependent material properties of which are assumed to be  $\nu_s = 0.48$  and  $E_s = (3.22 - 0.0034T)$  GPa in which  $T = T_0 + \Delta T$  and  $T_0 = 300$  K (room temperature) (Kolahchi *et al.* 2016a).

The effect of distribution type of CNT in layers of sandwich plates on the dimensionless buckling load ( $P = p / E_{11}^m h$ ) of system versus spring constant of elastic medium is presented in Fig. 2. The CNT uniform distribution and three types of FG patterns namely as FGV, FGO and FGX are considered. It can be seen that the buckling load increases with increasing the spring constant of elastic medium. It is since increasing the spring constant of elastic medium leads to stiffer structure. With respect to the distribution types of CNTs in the sandwich plate, it can be concluded that the FGX pattern is the best choice compared to other cases. It is because, in the FGX mode, the buckling load is maximum which means the stiffness of system is higher with respect to other three patterns. Meanwhile, the buckling load of structure with CNT uniform distribution is

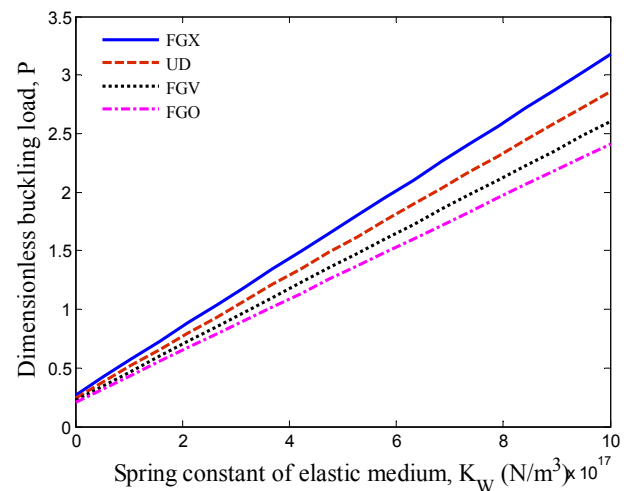


Fig. 2 CNTs distribution type effects on the variation of dimensionless buckling load versus spring constant of elastic medium

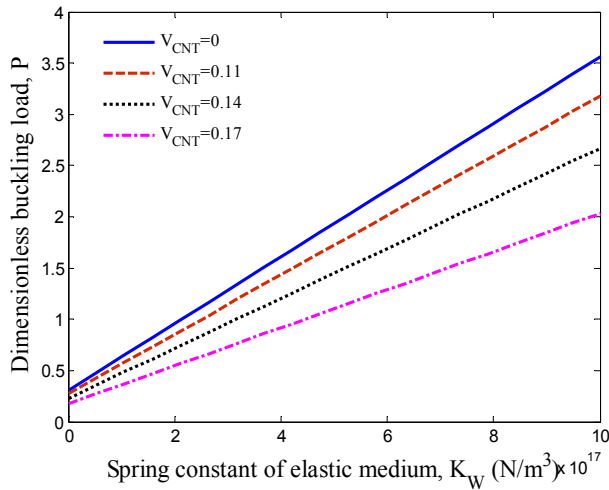


Fig. 3 CNTs volume percent effects on the variation of dimensionless buckling load versus spring constant of elastic medium

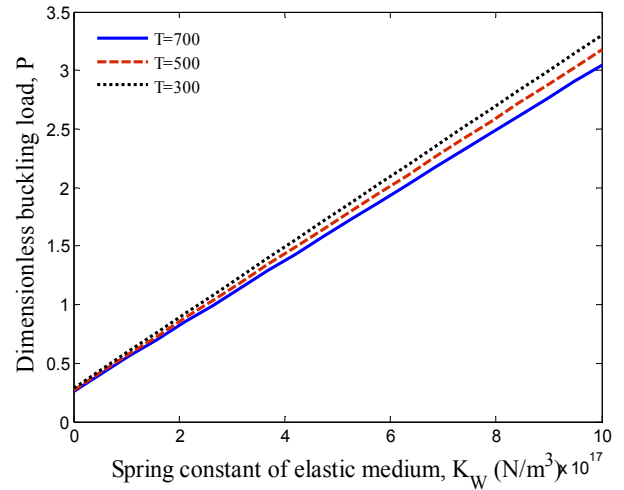


Fig. 5 Temperature change effects on the variation of dimensionless buckling load versus spring constant of elastic medium

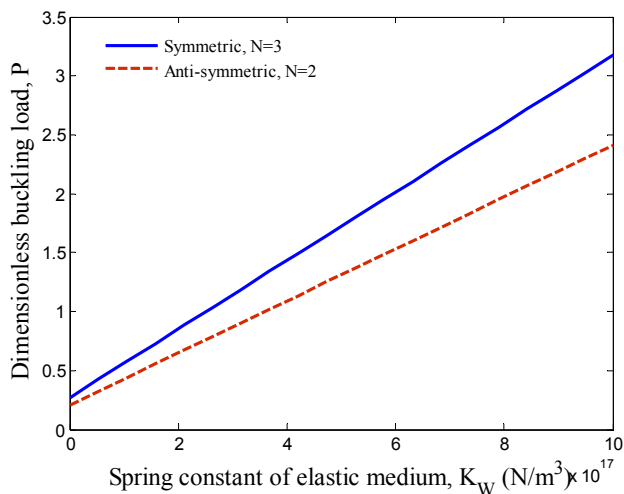


Fig. 4 Number of laminas effects on the variation of dimensionless buckling load versus spring constant of elastic medium

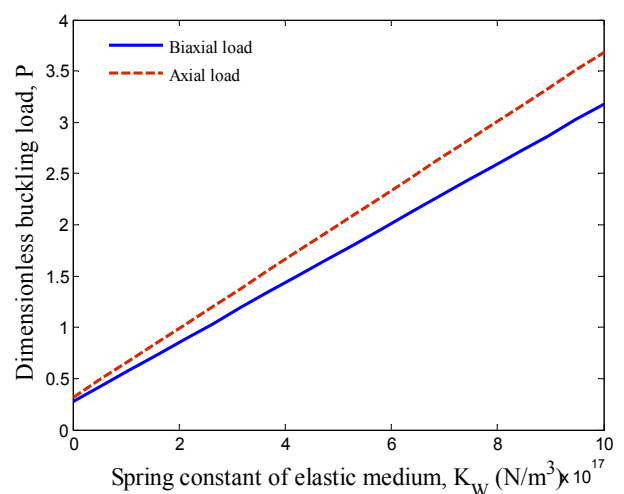


Fig. 6 Loading type effects on the variation of dimensionless buckling load versus spring constant of elastic medium

higher than FGV and FGO models. However, it can be concluded that the CNT distribution close to top and bottom are more efficient than those distributed nearby the mid-plane.

The effect of the CNT volume fraction on the dimensionless buckling load of the sandwich plate with respect to the spring constant of elastic medium is shown in Fig. 3. It can be found that increasing the CNT volume fraction increases the dimensionless buckling load of structure. This is due to the fact that the increase of CNT volume fraction leads to a harder structure. It is also concluded that the effects of CNT volume fraction becomes more prominent at higher spring constant of elastic foundation.

Fig. 4 illustrates the variation of the dimensionless buckling load versus the spring constant of elastic medium for the symmetric and anti-symmetric sandwich plate. It can be seen that in symmetric laminated composites (with three number of layers), the dimensionless buckling load

increases compared with the anti-symmetric ones (with two number of layers). The reason is that the symmetric laminated composite plates are more balance and stable.

The effect of temperature change on the dimensionless buckling load of the nanocomposite sandwich plate with respect to the spring constant of elastic medium is demonstrated in Fig. 5. The same as other figures, increasing the spring constant of elastic medium increases the dimensionless buckling load of the structure. It can be also found that the dimensionless buckling load of the structure decreases with increasing temperature change which is due to the higher stiffness of the nanocomposite sandwich plate with lower temperature.

Fig. 6 examines the influence of the loading types on the dimensionless buckling load of the structure versus the spring constant of elastic medium. Two types of loading include axial (along the  $x$  axis) and biaxial (along the  $x$  and  $y$  axes) are considered. As can be seen, in biaxial loading type the dimensionless buckling load is lower than axial

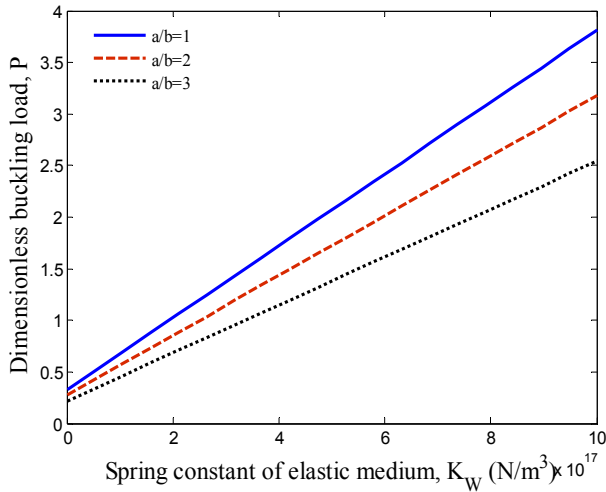


Fig. 7 Length to width ratio effects on the variation of dimensionless buckling load versus spring constant of elastic medium

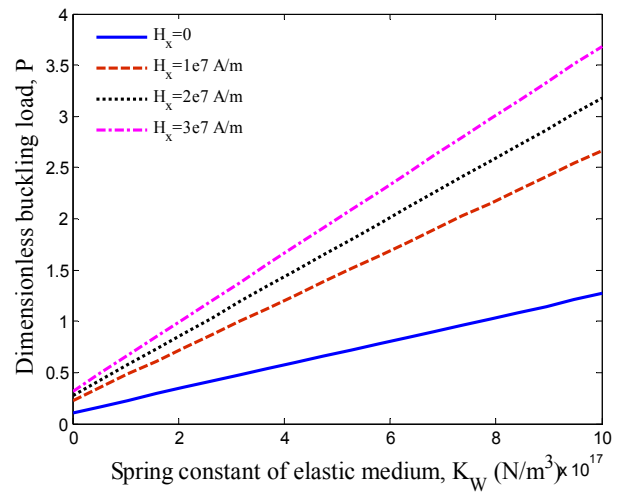


Fig. 9 Axial magnetic field effects on the variation of dimensionless buckling load versus spring constant of elastic medium

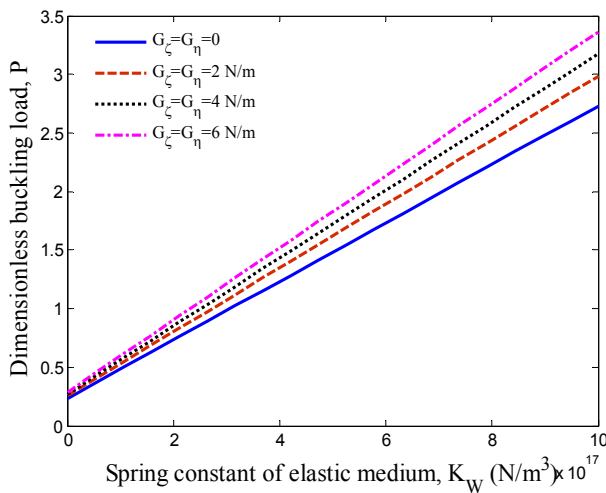


Fig. 8 Shear constant of elastic medium effects on the variation of dimensionless buckling load versus spring constant of elastic medium

loading type. The reason is that, in biaxial loading type, the load which applied to the edges is higher than the axial loading type and therefore the buckling of the structure occurs sooner. Also the effect of loading type is apparent in higher spring constant of elastic medium.

The effect of the length to width ratio ( $a/b$ ) on the dimensionless buckling load with respect to the spring constant of elastic medium is depicted in Fig. 7. As can be seen, the dimensionless buckling load of the sandwich plate decreases with increasing length to width ratio. It is because that increasing length to width ratio leads softer structure. Meanwhile, the effect of length to width ratio on the dimensionless buckling load becomes more prominent at higher spring constant of elastic medium.

The effect of the shear constant of elastic medium on the dimensionless buckling load versus spring constant of elastic medium is shown in Fig. 8. It can be observed that with increasing the shear and spring constants of elastic medium, the dimensionless buckling load is enhanced. It is

physically due to the fact that with increasing the shear and spring constants of elastic medium, the stiffness of the structure increases.

Fig. 9 demonstrated the effect of axial magnetic field on the variation of dimensionless buckling load versus spring constant of elastic medium. As can be seen, with increasing the axial magnetic field, the structure becomes stiffer and consequently, the dimensionless buckling load enhances.

## 5. Conclusions

In the present paper, based on Reddy shear deformation theory and Hamilton's principle, the governing equations of nanocomposite sandwich plates subjected to thermo-magneto-mechanical loadings were derived. Each layers of the sandwich structure was reinforced with FG-CNT and the corresponding effective material properties were obtained by Mixture rule. The structure was rested on the orthotropic temperature-dependent elastic medium. The problem of buckling of nanocomposite sandwich plates was then solved using an Navier method for the simply supported boundary conditions. The influences of different parameters such as the volume percent and distribution types of the CNTs, temperature change, elastic medium, magnetic field and geometrical parameters of the plates on the buckling load of the sandwich structure were investigated. It was found that the FGX pattern was the best choice compared to other case. Also, it was observed that increasing the CNT volume fraction increases the dimensionless buckling load of structure. It can be also found that the dimensionless buckling load of the structure decreases with increasing temperature change. In addition, with increasing the shear and spring constants of elastic medium, the dimensionless buckling load was enhanced. Furthermore, with increasing the axial magnetic field, the structure becomes stiffer and consequently, the dimensionless buckling load enhances.

## References

- Afsharmanesh, B., Ghaeheri, A. and Taheri-Behrooz, F. (2014), "Buckling and vibration of laminated composite circular plate on Winkler-type foundation", *Steel Compos. Struct., Int. J.*, **17**(1), 1-19.
- Akhavan, H., Hosseini Hashemi, Sh., Rokni Damavandi Taher, H., Alibeigloo, A. and Vahabi, Sh. (2009), "Exact solutions for rectangular Mindlin plates under in-plane loads resting on Pasternak elastic foundation. Part I: Buckling analysis", *Comput. Mat. Sci.*, **44**(3), 968-978.
- Chen, Ch.Sh., Tsai, T.Ch., Chen, W.R. and Wei, Ch.L. (2013), "Dynamic stability analysis of laminated composite plates in thermal environments", *Steel Compos. Struct., Int. J.*, **15**(1), 57-79.
- Dash, P. and Singh, B.N. (2012), "Buckling and post-buckling of laminated composite plates", *Mech. Res. Commun.*, **46**, 1-7.
- Gupta, S.S., Patel, B.P. and Ganapathi, M. (2003), "Nonlinear dynamic buckling of laminated angle-ply composite spherical caps", *Struct. Eng. Mech., Int. J.*, **15**(4), 463-476.
- Javed, S., Viswanathan, K.K., Aziz, Z.A., Karthik, K. and Lee, J.H. (2016), "Vibration of antisymmetric angle-ply laminated plates under higher order shear theory", *Steel Compos. Struct., Int. J.*, **22**(6), 1281-1299.
- Kiani, Y. (2016), "Buckling of FG-CNT-reinforced composite plates subjected to parabolic loading", *Acta Mech.*, 1-17.
- Kolahchi, R., Rabani Bidgoli, M., Beygipoor, Gh. and Fakhar, M.H. (2015), "A nonlocal nonlinear analysis for buckling in embedded FG-SWCNT-reinforced microplates subjected to magnetic field", *J. Mech. Sci. Tech.*, **29**(9), 3669-3677.
- Kolahchi, R., Safari, M. and Esmailpour, M. (2016a), "Dynamic stability analysis of temperature-dependent functionally graded CNT-reinforced visco-plates resting on orthotropic elastomeric medium", *Compos. Struct.*, **150**, 255-265.
- Kolahchi, R., Hosseini, H. and Esmailpour, M. (2016b), "Differential cubature and quadrature-Bolotin methods for dynamic stability of embedded piezoelectric nanoplates based on visco-nonlocal-piezoelectricity theories", *Compos. Struct.*, **157**, 174-186.
- Kolahchi, R., Zarei, M.Sh., Hajmohammad, M.H. and Naddaf Oskouei, A. (2017), "Visco-nonlocal-refined Zigzag theories for dynamic buckling of laminated nanoplates using differential cubature-Bolotin methods", *Thin-Wall. Struct.*, **113**, 162-169.
- Lee, S.Y. and Park, D.Y. (2007), "Buckling analysis of laminated composite plates containing delaminations using the enhanced assumed strain solid element", *Int. J. Solids Struct.*, **44**(24), 8006-8027.
- Lei, Z.X., Zhang, L.W. and Liew, K.M. (2016a), "Vibration of FG-CNT reinforced composite thick quadrilateral plates resting on Pasternak foundations", *Eng. Anal. Bound. Elem.*, **64**, 1-11.
- Lei, Z.X., Zhang, L.W. and Liew, K.M. (2016b), "Buckling of FG-CNT reinforced composite thick skew plates resting on Pasternak foundations based on an element-free approach", *Appl. Math. Comput.*, **266**, 773-791.
- Madani, H., Hosseini, H. and Shokravi, M. (2016), "Differential cubature method for vibration analysis of embedded FG-CNT-reinforced piezoelectric cylindrical shells subjected to uniform and non-uniform temperature distributions", *Steel Compos. Struct., Int. J.*, **22**(4), 889-913.
- Mayandi, K. and Jeyaraj, P. (2015), "Bending, buckling and free vibration characteristics of FG-CNT-reinforced polymer composite beam under non-uniform thermal load", *Proceed. Inst. Mech. Eng., Part L*, **229**(1), 13-28.
- Norouzi, H. and Younesian, D. (2016), "Nonlinear vibration of laminated composite plates subjected to subsonic flow and external loads", *Steel Compos. Struct., Int. J.*, **22**(6), 1261-1280.
- Reddy, J.N. (1984), "A simple higher order theory for laminated composite plates", *J. Appl. Mech.*, **51**(4), 745-752.
- Singh, S.K. and Chakrabarti, A. (2012), "Buckling analysis of laminated composite plates using an efficient C0 FE model", *Lat. Am. J. Solids Struct.*, **9**(3), 1-15.
- Singh, S., Singh, J. and Shukla, K.K. (2013), "Buckling of laminated composite plates subjected to mechanical and thermal loads using meshless collocations", *J. Mech. Sci. Tech.*, **27**(2), 327-336.
- Wang, H., Chen, Ch.S. and Fung, Ch.P. (2013), "Hygrothermal effects on dynamic instability of a laminated plate under an arbitrary pulsating load", *Struct. Eng. Mech., Int. J.*, **48**(1), 34-46.
- Yang, J., Ke, L.L. and Feng, Ch. (2015), "Dynamic buckling of thermo-electro-mechanically loaded FG-CNTRC beams", *Int. J. Str. Stab. Dyn.*, **15**(8), 1540017.
- Yas, M.H. and Heshmati, M. (2012), "Dynamic analysis of functionally graded nanocomposite beams reinforced by randomly oriented carbon nanotube under the action of moving load", *Appl. Math. Model.*, **36**(4), 1371-1394.
- Zhang, L.W. and Liew, K.M. (2015), "Large deflection analysis of FG-CNT reinforced composite skew plates resting on Pasternak foundations using an element-free approach", *Compos. Struct.*, **132**, 974-983.

CC